Microphysical Interpretation of Multi-Parameter Radar Measurements in Rain. Part II: Estimation of Raindrop Distribution Parameters by Combined Dual-Wavelength and Polarization Measurements

A. R. JAMESON

Illinois State Water Survey, Champaign, IL 61820

(Manuscript received 8 November 1982, in final form 25 March 1983)

ABSTRACT

The radar reflectivity weighted mean axis ratio $\bar{\mathcal{R}}$ and the variance of the axis ratio distribution $\sigma^2_{\mathcal{R}}$ of an ensemble of raindrops can be estimated from polarization radar measurements. If the shape function relating axis ratio to drop size is known or measured, then these quantities may be transformed into the radar reflectivity weighted mean diameter $\bar{\mathcal{D}}$ and, in the case of quiescent drops, into the variance of the raindrop size distribution $\sigma^2_{\mathcal{D}}$. Although these parameters are of intrinsic meteorological interest, estimates of the rainfall rate in still air R_0 and of liquid water content W can also be constructed. In principle, estimates using both $\bar{\mathcal{D}}$ and $\sigma^2_{\mathcal{D}}$ appear, potentially, to be more accurate than estimates based only on $\bar{\mathcal{D}}$. Realization of this potential improvement probably depends on the development of techniques to extract that component of $\sigma^2_{\mathcal{R}}$ arising solely from the raindrop size distribution.

1. Introduction

The desire for more complete qualitative and quantitative descriptions of rain using radars has spurred the development of techniques which use several radar parameters measured simultaneously. Multiple wavelength techniques involving simultaneous measurements at attenuating and non-attenuating wavelengths have been proposed and developed (Atlas, 1954; Wexler and Atlas, 1963; Eccles and Mueller, 1971; Atlas and Ulbrich, 1974; Atlas and Ulbrich, 1977; Ulbrich and Atlas, 1978). Similarly, radar polarization techniques have been proposed and used to more accurately characterize the properties of rain (McCormick *et al.*, 1972; Hendry and McCormick, 1974; McCormick and Hendry, 1975; Hendry *et al.*, 1976; McCormick and Hendry, 1976; Seliga and Bringi, 1976; Hall *et al.*, 1980; Goddard *et al.*, 1982).

Since multiple wavelength and polarization measurements each require relatively sophisticated radar systems, only recently have both techniques been applied simultaneously in a study of the bright band (Humphries and Barge, 1979). This paper considers the microphysical information which can be obtained through the simultaneous use of both techniques in studies of rain.

In another paper (Jameson, 1983a) it was shown that the radar reflectivity weighted axis ratio ($\bar{\mathcal{R}}$) can be deduced from differential reflectivity (Z_{DR}) measurements (Seliga and Bringi, 1976) or from the combined measurements of the circular depolarization ratio (Γ) and the magnitude of the cross-correlation of the two orthogonally circularly polarized channels (ρ) (McCormick *et al.*, 1972). In addition, Γ and ρ can be manipulated to produce a radar reflectivity weighted estimate of the variance $\sigma^2_{\mathcal{R}}$ of the axis ratio. Of more direct meteorological interest, however, are the estimates of $\bar{\mathcal{D}}$ and $\sigma^2_{\mathcal{D}}$, the first and second radar power weighted moments of the raindrop size distribution. In particular, $\bar{\mathcal{D}}$ can be used to estimate rainwater content (W) and rainfall rate in still air (R_0). If $\sigma^2_{\mathcal{D}}$ is also known, then estimates of W and R_0 can be significantly improved over estimates based on $\bar{\mathcal{D}}$ alone. The central purpose of this paper is to show that $\bar{\mathcal{R}}$ and $\sigma^2_{\mathcal{R}}$ can often be directly related to $\bar{\mathcal{D}}$ and $\sigma^2_{\mathcal{D}}$ through a shape function which can be estimated from simultaneous dual-wavelength and polarization measurements.

At longer radar wavelengths (greater than ~3 cm), raindrops are largely in the Rayleigh scattering region. In that case the polarization properties of rain are determined by shape alone. In order to relate drop shapes to drop sizes, it is necessary to define a "shape function." If drop shapes are characterized as oblates or prolates, the shape function relates a specific axis ratio to a specific equivalent spherical drop diameter D. In the case of an ensemble of identically sized drops distributed over a variety of axis ratios, the shape function can then be defined as a relationship between the mean axis ratio $\bar{r}$ and the drop size. In the most general case of an ensemble of differently shaped and differently sized drops, the shape function relates the mean axis ratio to the mean drop size.

In this paper, a dual-wavelength (10.71 and 3.21 cm wavelengths) estimator of $\bar{\mathcal{D}}$ is formulated. In conjunction with $\bar{\mathcal{R}}$, $\bar{\mathcal{D}}$ is then used to define the pa-

rameters in a simple but general form of the shape function. This permits the conversion of σ_R^2 to σ_D^2.

2. The drop shape function

a. Linear form of the shape function

Unfortunately, little is known about the drop shape function in the atmosphere above the surface layer or about possible changes in the shape function under various meteorological conditions. Wind tunnel studies of individual drops under conditions of laminar flow (Pruppacher and Beard, 1970) and turbulent flow (Brook and Latham, 1968), both suggest linear relations between $\bar{r}$ and D even though the suggested relations are different from each other. Photographic studies of drop shape at ground level also show variable, but nearly linear, shape functions (Bresch, 1982). Figure 1 is a plot of linear fits to observed mean axis ratios at four locations (adapted from Bresch, 1982) along with the correlation coefficients associated with each fit. These measurements represent long time averages under a variety of meteorological and geographical settings. Although "instantaneous" shape functions may differ from these long term averages, it appears that a simple relationship

$$\bar{r} = a - bD \tag{1}$$

may perform adequately as a general form of a shape function for raindrops. It is also easy to show from (1) that for a drop size distribution, the reflectivity weighted mean quantities are related by

$$\bar{\mathcal{R}} = a - b\bar{\mathcal{D}}. \tag{2}$$

In the remainder of this work, (1) and (2) will be used. This assumption, however, is not crucial. If subsequent investigations lead to more refined shape functions, alternative conversions of $\bar{\mathcal{R}}$ and σ_R^2 to estimates of $\bar{\mathcal{D}}$ and σ_D^2 can be found, in principle, so long as the correspondence between $\bar{r}$ and D remains one-to-one.

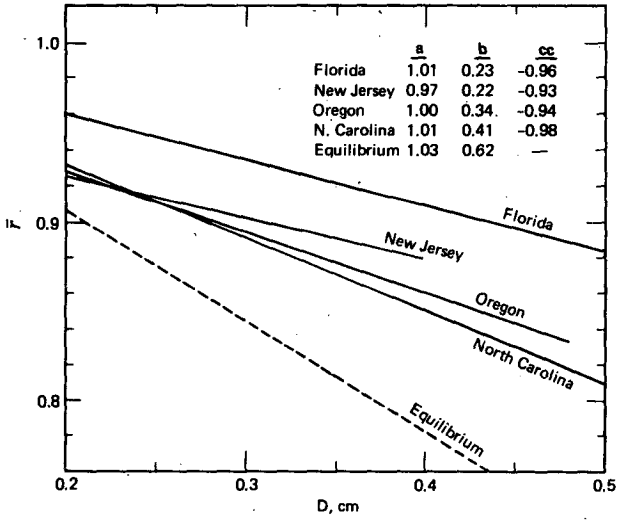

FIG. 1. Linear fits of mean axis ratio $\bar{r}$ as a function of D from photographs of drops at the indicated locations. The intercept (a), slope (b), and correlation coefficient (cc) are given.

In the atmosphere, the shape function may vary considerably under different meteorological conditions. For example, during light rain, when raindrop collisions are relatively infrequent, or during the melting of ice, when air bubbles or unmelted remnants may damp the natural oscillations of the drop, the raindrop shapes may be nearly those at equilibrium. In this case the coefficient b in (1) and (2) should be approximately 0.62. In other circumstances, some raindrops may be oscillating as a result of turbulence, wind shear or collisions with other drops in more intense rains (Beard *et al.*, 1983). Since some modes of oscillation appear to bias the mean shape from equilibrium toward unity (Jameson and Beard, 1982; Beard *et al.*) and since from collisions, for example, large drops would generally be expected to oscillate more than small drops (see Beard *et al.*), larger drops might be expected to have mean axis ratios more offset from equilibrium than are the axis ratios of smaller drops. This should lead to values of b less than 0.62 (see Fig. 1).

b. Estimation of the linear shape function

The estimation of a linear shape function requires some means of determining both a and b in (1) and (2). At some sufficiently small drop size D_s (say 0.05 cm) $\bar{r}$ can be assumed to be near unity and

$$a = 1 + bD_s. \tag{3}$$

In addition if $\bar{\mathcal{R}}$ is estimated from polarization measurements, then using (2) and (3) we have

$$\left.\begin{aligned} b &= \frac{(1 - \bar{\mathcal{R}})}{(\bar{\mathcal{D}} - D_s)} \\ a &= \bar{\mathcal{R}} + b\bar{\mathcal{D}} \end{aligned}\right\}. \tag{4}$$

All that is required to implement (4), then, is a measure of $\bar{\mathcal{D}}$. At longer radar wavelengths and with current technology, at least, polarization power measurements alone provide raindrop shape information only. They cannot yet provide direct estimates of $\bar{\mathcal{D}}$ without *a priori* assumptions about the very shape function that we are trying to determine. Although at shorter wavelengths, polarization measurements affected by Mie scattering may possibly provide some clues about drop size, such measurements would be of limited usefulness since propagation effects would tend to rapidly degrade the signal in more intense rainfall.

Alternatively, at shorter wavelengths, the attenuation rate (A) is a strong function of drop size. At a wavelength of 3.2 cm, Atlas and Ulbrich (1974)

showed that the attenuation cross-section σ_A of a spherical drop was related to the diameter by approximately $D^{4.46}$. On the other hand at 10.71 cm wavelength the backscatter cross-section $\sigma_B \propto D^6$. Therefore, the quantity σ_B/σ_A varies approximately as $D^{1.54}$ or, conversely, $D \propto (\sigma_B/\sigma_A)^{0.649}$. For a distribution of drops then

$$\left.\begin{aligned} \frac{A}{Z} &\propto \frac{\int \sigma_A N_D dD}{\int \sigma_B N_D dD} \\ \frac{A}{Z} &\propto \frac{\int \sigma_B D^{-1.54} N_D dD}{\int \sigma_B N_D dD} \\ \frac{A}{Z} &\propto \overline{\mathcal{D}^{-1.54}} \end{aligned}\right\}, \tag{5}$$

where $\mathcal{D}$ denotes a radar reflectivity weighted diameter, A the one way attenuation rate (dB km^{-1}) at 3.2 cm wavelength, and Z is the reflectivity factor (mm^6 m^{-3}) at 10 cm wavelength. This equation suggests that a possible estimate of $\bar{\mathcal{D}}$ might take the form

$$\bar{\mathcal{D}} = C(\chi)^{\beta}, \tag{6}$$

where $\chi = Z/A$, and C and β are constants with $\beta \approx 0.65$. Since (5) and (6) do not depend on any particular form of the drop size distribution, the constant and power of χ in (6) should be widely applicable.

In order to evaluate the constants in (6), calculations were performed for a wide variety (see Section 4 of Jameson, 1983a) of drop size and drop shape distributions. A least square fit of χ as a function of $\bar{\mathcal{D}}$ was calculated. From values of 10 cm reflectivity factor calculated for horizontal linear polarization and the 3 cm attenuation rate corresponding to horizontal transmission, we have

$$\bar{\mathcal{D}} = (2.303 \times 10^{-4})\chi^{0.639}, \tag{7}$$

with a correlation coefficient of 0.98. In these computations the associated standard error of the estimate is 0.028 cm. The exponent of χ is quite close to the anticipated value.

Similar expressions may be derived for vertical linear polarizations, i.e.,

$$\bar{\mathcal{D}} = (8.684 \times 10^{-5})\chi^{0.737}, \tag{8}$$

where the correlation coefficient is 0.96 and the standard error of the estimate is 0.036 cm. For horizontal linear polarization at the 10 cm wavelength and vertical polarization at 3 cm,

$$\bar{\mathcal{D}} = (5.251 \times 10^{-4})\chi^{0.556}, \tag{9}$$

where the correlation coefficient is 0.97 and the standard error of the estimate is 0.037 cm.

Although (7) is likely to be adequate for many uses, a more accurate representation of the dependence of $\bar{\mathcal{D}}$ on χ can be obtained by a 3-piece power law fit given by

$$\left.\begin{aligned} \bar{\mathcal{D}} &= (4.680 \times 10^{-4})\chi^{0.566}, \\ &\qquad \log_{10}(\chi) \leqslant 4.784 \\ \bar{\mathcal{D}} &= (9.139 \times 10^{-6})\chi^{0.935}, \\ &\qquad 4.784 < \log_{10}(\chi) \leqslant 4.922 \\ \bar{\mathcal{D}} &= (2.833 \times 10^{-3})\chi^{0.427}, \\ &\qquad 4.922 < \log_{10}(\chi) \end{aligned}\right\}. \tag{10}$$

The corresponding standard error of the estimate is 0.016 cm. These equations, which better account for the variation of attenuation cross-section with diameter than does a single power law fit, produce smaller deviations of the estimate from the true $\bar{\mathcal{D}}$.

In Table 1, the mean diameter estimated from (10), $\bar{\mathcal{D}}_e$, is compared to the actual values, $\bar{\mathcal{D}}_m$, corresponding to each particular drop size distribution example. In these examples, $\bar{\mathcal{D}}_e$ is within 6% of $\bar{\mathcal{D}}_m$ with the single exception being the bimodal distribution having equal contributions to the radar reflectivity

TABLE 1. Comparison of actual and estimated $\bar{\mathcal{D}}$ for several drop size distributions.

	D_{max} (cm)	D_{min} (cm)	Λ (cm^{-1})	N_D (cm^{-4})	$\bar{\mathcal{D}}_m$ (cm)	$\bar{\mathcal{D}}_e$ Eq. (10)	a_{est}	b_{est}
Exponential								
$N_D = N_0 \exp(-\Lambda D)$	0.6	0.01	20.0	1.85×10^{-1}	0.340	0.330	1.03	0.59
Gamma								
$N_D = N_0 D^2 \exp(-\Lambda D)$	0.6	0.01	20.0	1.49	0.409	0.393	1.03	0.60
Gaussian-like								
$N_D = N_0/D \exp(-\Lambda^2 D^2)$	0.6	0.01	10.0	9.82×10^{-2}	0.170	0.160	1.03	0.56
Rectangular								
$N_D = N_0$	0.6	0.01	0	2.37×10^{-5}	0.530	0.516	1.03	0.61
Monodisperse	0.30	0.30	0	1.85×10^{-2}	0.300	0.315	1.03	0.55
Bimodal	0.60	0.10	—	Equal power	0.371	0.169	1.06	1.26
Bimodal	0.60	0.10	—	Equal concentration	0.600	0.595	1.03	0.60

from 0.1 and 0.6 cm drops. Although this may be an unrealistic raindrop distribution it does present an example of a situation when (10) would clearly fail.

By invoking any of the relations (7)–(10), the intercept (a) and slope (b) of a linear shape relation may be calculated from (4). Seven examples are presented in Table 1. In these examples, the drops were assumed to be approximately equilibrium shape ($\bar{r} = 1.03 - 0.62D$) with Gaussian axis ratio distributions (Jameson, 1983a). In these computations of a and b, D_s was assumed to be 0.05 cm. This choice is somewhat arbitrary. If D_s were increased to 0.07 cm, however, b would increase by no more than +0.1 although the intercept would increase by +0.02 or more to values (1.04–1.06) well beyond those expected for equilibrium drops (1.03) or those encountered in the drop camera data.

Most estimates of b in Table 1 are within about −0.07 to −0.01 of the actual value (0.62), while the intercept was within less than ±0.005 of 1.03. The one exception occurred again with the equal-power bimodal distribution. As previously discussed, the algorithm (10) for $\bar{\mathcal{D}}$ fails for this distribution, and (4) subsequently leads to unrealistic values of a and b. In general, at locations where b appears to exceed 0.62 analysis results should be viewed with caution.

3. Meteorological Interpretation of $\bar{\mathcal{D}}$ and $\sigma^2_{\mathcal{D}}$

One of the long standing goals of radar meteorology has been to describe, to some degree, the properties of the raindrop distribution. This is particularly elusive since incoherent radars measure only a limited number of reflectivity weighted integrated properties or moments of a drop size distribution.

Polarization and dual-wavelength radar techniques can apparently provide radar power weighted estimates of both the mean and variance of the drop size distribution. Specifically, the shape function permits the transformation of $\bar{\mathcal{R}}$ and $\bar{\mathcal{D}}$. Similarly, insofar as a linear shape function is applicable

$$\sigma^2_{\mathcal{D}} = \sigma^2_{\mathcal{R}} b^{-2}. \tag{11}$$

This information, however, is not necessarily adequate to distinguish between the many forms of drop size distributions that have been suggested. For example, many meteorological drop size distributions tend to exhibit decreasing number concentrations with increasing size. Since, at long wavelengths, the radar reflectivity weighting is proportional to D^6, the resultant radar reflectivity weighting functions applicable to $\bar{\mathcal{D}}$ and $\mathcal{D}^2$ will usually have a strong peak with a trailing tail at larger diameters. The most telltale identifier of various distribution forms might, in all likelihood, be the skewness, μ_3 (third moment), and perhaps higher moments of the radar reflectivity weighted drop size distribution (e.g., Fig. 2a).

For many drop size distributions, μ_3 is small indicating that many radar weighting functions are essentially symmetric. Over a wide variety of drop size distributions (see Section 4 of Jameson, 1983a) the largest value of $|\mu_3|$ was only 0.03 cm^3. Many radar weighting functions are, therefore, predominately symmetric and, as such, are fairly completely described by $\bar{\mathcal{D}}$ and $\sigma^2_{\mathcal{D}}$. Consequently, however, different forms of many drop size distributions will be indistinguishable using measurements of only $\bar{\mathcal{D}}$ and $\sigma^2_{\mathcal{D}}$.

As an example, in Fig. 2a, the radar weighting functions for $\bar{\mathcal{D}}$, normalized to have the same peak value, are shown for an exponential, gamma and Gaussian-like drop size distributions. Even though each distribution is unique, the peaks in the radar weighting functions for $\bar{\mathcal{D}}$ are all at 0.3 cm. The resulting values of $\bar{\mathcal{D}}$ are essentially identical. In this sense, with re-

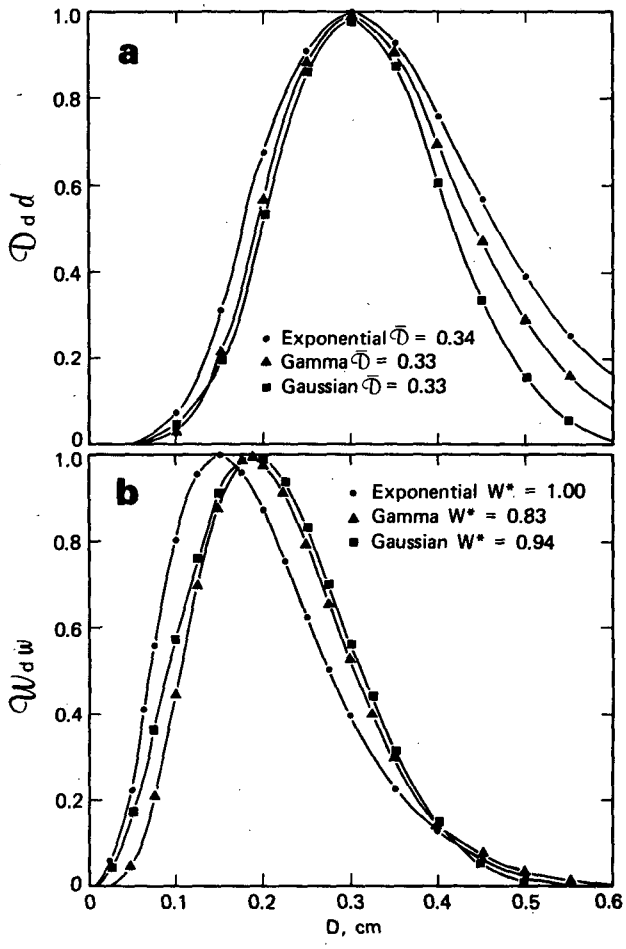

FIG. 2. (a) A plot of the density distribution $\mathcal{D}d_d$ for the reflectivity weighted mean diameter $\mathcal{D}$ for three different drop size distributions with peaks at 0.3 cm. The curves are normalized to their respective peak values. The corresponding $\bar{\mathcal{D}}$ are given. (b) The liquid water content distribution function $\mathcal{W}d_w$ corresponding to the three drop size distribution in Fig. 2a. The curves have been normalized to their respective peak values. W^* is the total water content (g m^{-3}) corresponding to each drop size distribution.

spect to the radar, the three drop size distributions are nearly equivalent. To rephrase, for any particular radar weighting function, such as in Fig. 2a, there are frequently several drop size distributions which could have been used to generate it. Although this may be unfortunate if attempting to distinguish between different drop size distributions, this relative insensitivity to many particular forms of the drop size distribution has important implications for the estimation of rain water content W and the rainfall rate in still air R_0 from $\bar{\mathcal{D}}$.

In principle, R_0 and W can be derived from $\bar{\mathcal{D}}$. For an exponential distribution, for example,

$$\left.\begin{aligned} \bar{\mathcal{D}} &\propto \frac{1}{\Lambda} \\ W &\propto \frac{1}{\Lambda^4} \\ R_0 &\propto \frac{1}{\Lambda^{4+\beta}} \end{aligned}\right\}, \tag{12}$$

so that

$$\left.\begin{aligned} W &\propto \bar{\mathcal{D}}^4 \\ R_0 &\propto \bar{\mathcal{D}}^{4+\beta} \end{aligned}\right\}, \tag{13}$$

where β is the exponent in an approximate power law relating drop diameter to terminal fall speed. Relations similar to (12) and (13) hold for other analytic expressions of drop size distributions as well. Here R_0 and W do depend somewhat more strongly on the form of the drop size distribution, however, than does the radar weighting function for $\bar{\mathcal{D}}$. In Fig. 2b, for example, the water content distribution function for the same drop distributions used in Fig. 2a are shown. Although these functions are quite similar, there are differences which produce variations in the total water content (W^*) which ranges from 1.00 to 0.83 g m^{-3}.

An additional source of variation of estimates of R_0 and W founded on $\bar{\mathcal{D}}$ alone is implicit in (12)–(13). Although the dependence of R_0 and W on $\bar{\mathcal{D}}$ is evident, the precise equation for this relationship depends on the proportionality constants. These constants, in part, depend on N_0, the limiting drop concentration as D goes to zero. This component is usually accounted for by using the reflectivity factor, however. The constants also depend, though, upon the variance of the drop size distribution or, alternatively, upon the minimum ($D_{\min}$) and maximum ($D_{\max}$) diameters of the drop size distribution. Depending upon various combinations of $D_{\min}$ and $D_{\max}$, the proportionality constants will vary considerably. Consequently, this will introduce a range of values of W and R_0 for any particular $\bar{\mathcal{D}}$.

In order to investigate the magnitudes of variations in R_0 and W introduced by different forms of drop size distributions and different combinations of $D_{\min}$ and $D_{\max}$, a large number of computations were performed using exponential, gamma, and Gaussian-like drop size distributions. The slope parameters in these distributions varied from 0 to 50 cm^{-1} (cm^{-2} for the Gaussian distribution) while $D_{\max}$ ranged from 0.10 to 0.60 cm and $D_{\min}$ varied from 0.01 to $D_{\max}$. Both monodisperse and uniform drop size distributions were, therefore, included in the computations which encompassed over 500 000 different drop size distributions. In addition, a range of shape functions bounded by the equilibrium curve and another lying somewhat above the Miami curve (Fig. 1) were used. The radar wavelength was 10.71 cm and back-scatter cross-sections were computed using the Gans (1912) approximation.

In Fig. 3, for a constant reflectivity factor [40 dB(Z)], the average values of R_0 corresponding to each $\bar{\mathcal{D}}$ are shown for the three different forms of the drop size distribution. This average is the arithmetic mean of the largest and smallest rainfall rates found at each $\bar{\mathcal{D}}$ in the computations. The variation in average R_0 is generally less than about ±20% of the values corresponding to the gamma drop size distributions. Combining the results for exponential,

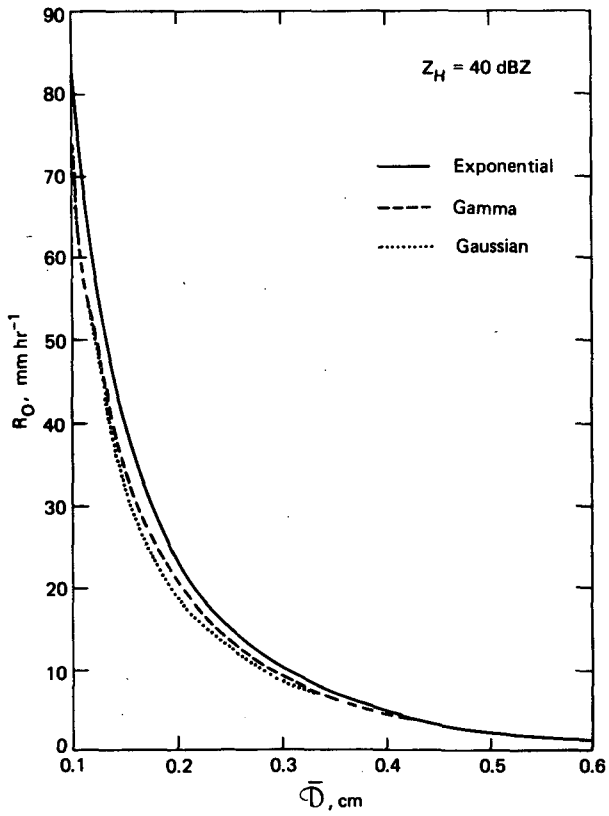

FIG. 3. The average rainfall rate in still air, R_0, as a function of mean power weighted drop diameter $\bar{\mathcal{D}}$ for three different forms of drop size distributions. The curves are based on calculations for several hundred thousand individual drop size distributions. All values are normalized to a reflectivity factor of 40 dB(Z).

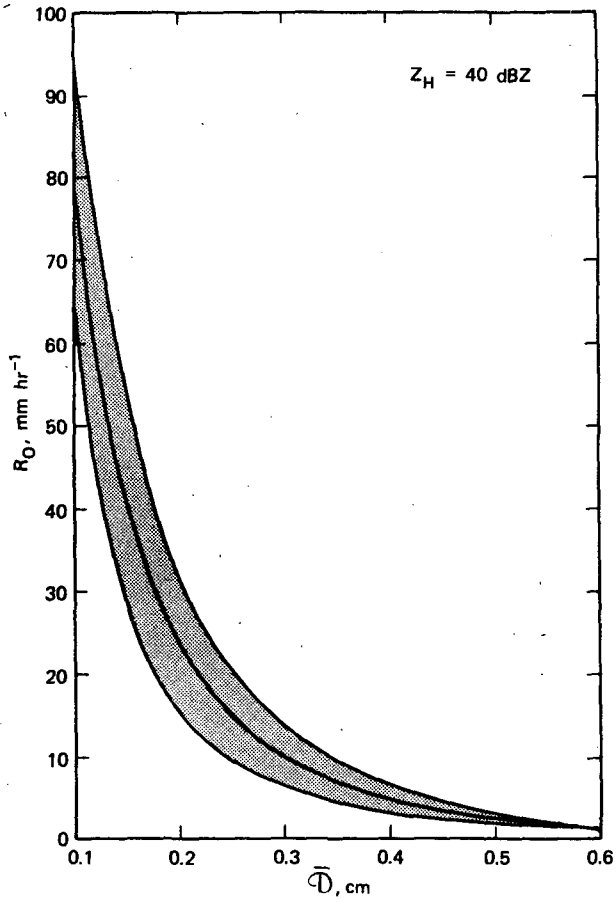

FIG. 4. The middle curve is the average rainfall rate in still air R_0 for the same distributions used in deriving Fig. 3. The upper and lower curves delineate the maximum and minimum excursion of rainfall rate about R_0. All numbers are scaled to a reflectivity factor of 40 dB(Z).

gamma, and Gaussian-like drop size distributions leads to Fig. 4. The upper and lower curves delineate the maximum and minimum values of R_0. These values are at most ±36% of the overall average values of R_0 and is well represented (correlation coefficient = −0.997) by a two piece power law given by

$$\left.\begin{aligned} R_0 &= (1.048 \times 10^{-4})10^{Z_H/10}\bar{\mathcal{D}}^{-1.905}, \\ &0.1 \leqslant \bar{\mathcal{D}} \leqslant 0.32 \text{ cm} \\ R_0 &= (3.352 \times 10^{-5})10^{Z_H/10}\bar{\mathcal{D}}^{-2.907}, \\ &0.32 < \bar{\mathcal{D}} \leqslant 0.6 \text{ cm} \end{aligned}\right\}. \quad (14)$$

Similar results for water content are shown in Fig. 5. The upper and lower values of W are at most ±54% of the overall average W (middle curve, Fig. 5). The greater range of W as compared to R_0 is probably due to the weaker dependence of W on diameter. Therefore, the variation in drop size distributions have a slightly stronger influence on W than R_0.

For W, a two piece power law also represents the overall average W quite well (correlation coefficient = −0.997). It takes the form

$$\left.\begin{aligned} W &= (2.361 \times 10^{-6})10^{Z_H/10}\bar{\mathcal{D}}^{-2.527}, \\ &0.1 \leqslant \bar{\mathcal{D}} \leqslant 0.31 \text{ cm} \\ W &= (6.957 \times 10^{-7})10^{Z_H/10}\bar{\mathcal{D}}^{-3.561}, \\ &0.31 < \bar{\mathcal{D}} \leqslant 0.6 \text{ cm} \end{aligned}\right\}. \quad (15)$$

Insofar as the drop size distributions used to develop (14) and (15) encompass naturally occurring raindrop size distributions, (14) and (15) may be applied to data to estimate R_0 and W. It should be remembered, however, that the constants in (14)–(15) will change somewhat with the use of more precise radar cross-sections than those derived from the Gans approximation. Estimates of $\bar{\mathcal{D}}$ can be obtained either from dual-wavelength radar data or from polarization

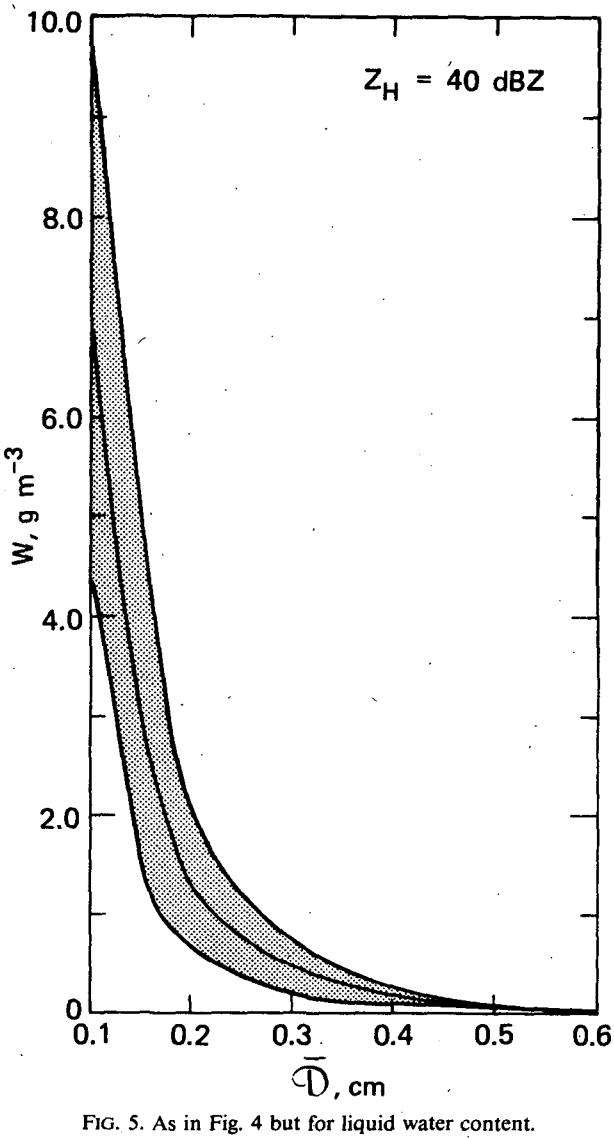

FIG. 5. As in Fig. 4 but for liquid water content.

measurements (Z_{DR} or the combination of Γ and ρ), provided the drop shape function is known.

Estimates of R_0 and W can potentially be improved, by using all of the meteorological information provided by measurements of both $\bar{\mathcal{D}}$ and $\sigma_{\mathcal{D}}^2$. Returning again to an exponential distribution, as an example, just as $\bar{\mathcal{D}}$ depends upon Λ, $D_{\max}$, $D_{\min}$, and N_0, so does $\sigma_{\mathcal{D}}^2$. Using the reflectivity factor to eliminate the dependence on N_0, as previously mentioned, the combination of $\bar{\mathcal{D}}$ and $\sigma_{\mathcal{D}}^2$ reduces the number of independent variables from three to one. There will be a similar reduction in the number of independent variables even for an ensemble of various forms of drop size distributions. The decreased number of independent variables leads to a reduction in the range of values of R_0 and W to be expected for a particular combination of $\bar{\mathcal{D}}$ and $\sigma_{\mathcal{D}}^2$. If available, a measure of μ_3, for example, would also further reduce the range of R_0 and W estimates.

Figure 6 is a plot of an average R_0 as a function of $\bar{\mathcal{D}}$ and $\sigma_{\mathcal{D}}$ calculated using the same ensemble of drop size distributions on various shape functions used previously to develop (14) and (15). From this collection of drop size distributions the minimum and maximum rainfall rates were determined as functions of $\bar{\mathcal{D}}$ and $\sigma_{\mathcal{D}}$. Then R_0 is defined as the arithmetic average of these minimum and maximum rainfall rates. In Fig. 6 the minimum and maximum values are expressed as percentage of the overall average R_0. Whereas in Fig. 4 the minimum and maximum rainfall rates were within ±36% of the mean rainfall rate when only $\bar{\mathcal{D}}$ was available the minimum and maximum rainfall rates in Fig. 6 are only ±14% of the average when both $\bar{\mathcal{D}}$ and $\sigma_{\mathcal{D}}$ are used. Generally the variations are less than that. Note that in Fig. 6 R_0 is scaled to a reflectivity factor of 40 dB(Z). Therefore, for Z_H = 50 dB(Z), R_0 should be multiplied by 10 while for Z_H = 30 dB(Z), R_0 should be one tenth of the value in Fig. 6.

Similarly, Fig. 7 illustrates the variation of the overall average of W as a function of $\bar{\mathcal{D}}$ and $\sigma_{\mathcal{D}}$. As before, the magnitudes of the variations exceed those for R_0, but now rather than maximum variations of ±54% (Fig. 5), they are reduced to at most ±35% over a rather limited domain.

In principle, then, use of both $\bar{\mathcal{D}}$ and $\sigma_{\mathcal{D}}^2$ can make a significant contribution to the estimation of R_0 and W. Table 2 illustrates the values anticipated for a number of different sample distributions.

As expected, use of both $\bar{\mathcal{D}}$ and $\sigma_{\mathcal{D}}$ produces better estimates of R_0 and W than use of $\bar{\mathcal{D}}$ alone. Even for the rather extreme case of a bimodal distribution in which 0.1 and 0.6 cm size drops contribute equally to the total reflectivity, Figs. 6–7 at least indicate that

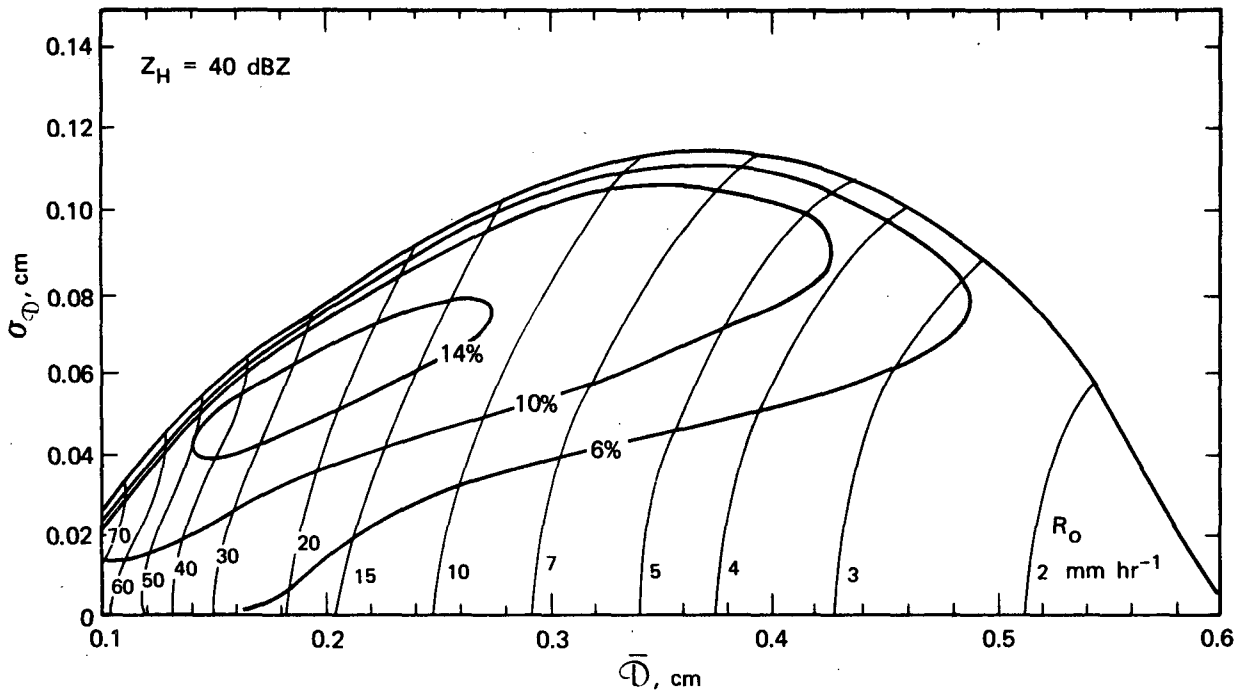

FIG. 6. The average rainfall rate, R_0, is plotted (thin lines) as a function of $\bar{\mathcal{D}}$ and $\sigma_{\mathcal{D}}$. R_0 is the arithmetic average of the minimum and maximum rainfall rates found in the calculations corresponding to each pair of $\bar{\mathcal{D}}$ and $\sigma_{\mathcal{D}}$. These maxima and minima are expressed as percentages of the mean. For example, if $\bar{\mathcal{D}}$ = 0.24 cm and $\sigma_{\mathcal{D}}$ = 0.058 cm, then R_0 = 15 mm h^{-1}. Since the corresponding percentage is ±14%, the maximum and minimum values would be approximately 17.1 and 12.9 mm h^{-1}, respectively. All values of R_0 are normalized to 40 dB(Z) (see text).

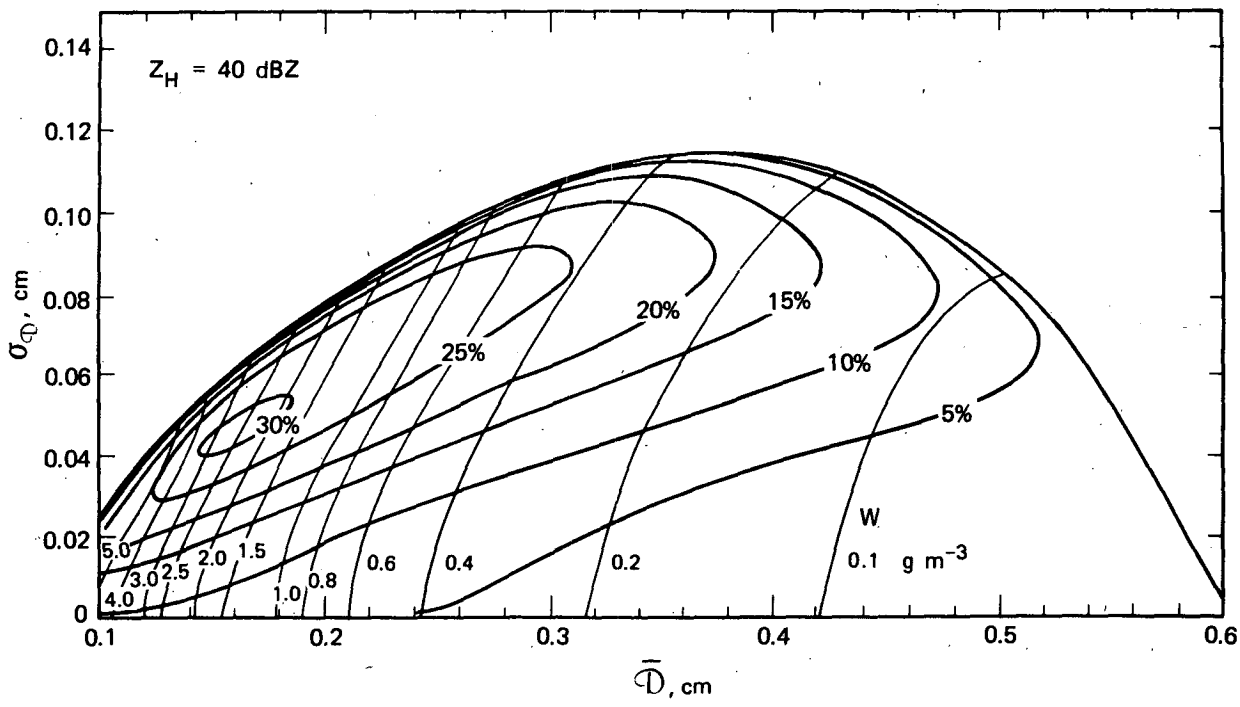

FIG. 7. As in Fig. 6 except it is for liquid water content W.

this distribution is "unusual," i.e., not represented by any exponential, Gaussian-like, gamma, rectangular, or monodisperse distribution. Measurements of only the first two reflectivity weighted moments of the drop size distribution do not adequately characterize this particular distribution. The skewness of that drop size distribution would be around -0.20 cm^3, a value far exceeding those expected for the distributions used to develop (14) and (15) and Figs. 6–7. Clearly a measure of skewness (or $\overline{\mathcal{D}^3}$) could have been used to detect the inapplicability of (14) and (15) and Figs. 6–7 for this particular distribution.

Although $\sigma_{\mathcal{D}}$ is of great potential use, determining its value is not necessarily simple if each size of raindrop exhibits a distribution of axis ratios such as might occur because of raindrop oscillation. Then, $\sigma_{\mathcal{R}}^2$ is composed of two components, one arising from the drop size distribution and one from the axis ratio distributions for each raindrop size. At times, one component may dominate the other while sometimes they may be equally important. For example, for an exponential drop size distribution consisting of drops up to 0.6 cm with $\Lambda = 20$ cm^{-1}, $\sigma_{\mathcal{R}}$ is calculated to be 0.0689, for equilibrium shaped drops. On the other hand, if the drop size distribution consisted of drops described by the Miami drop camera data (see Part I), $\sigma_{\mathcal{R}} = 0.0956$. If in both instances it is assumed that the slopes in the shape functions are known then in the first instance, (12) would imply $\sigma_{\mathcal{D}} = 0.111$, the true standard deviation, while in the latter instance, (12) would lead to $\sigma_{\mathcal{D}} = 0.416$ which is about 4 times the true standard deviation of the drop size distribution. In general, some method of accounting for the inflation of the measured $\sigma_{\mathcal{D}}$ beyond the value arising from the spread in the drop size distribution alone must be formulated if estimates of $\sigma_{\mathcal{D}}$ are to be

TABLE 2. Comparison of actual values of rainfall rate and rainwater content to various estimates.

	D_{max} (cm)	D_{min} (cm)	Λ (cm^{-1})	R_m (mm h^{-1})	R_e Eq. (14)	R_e Fig. 6	W_m (g m^{-3})	W_e Eq. (15)	W_e Fig. 7
Exponential	0.60	0.01	20	97.4	73.5	100.2	4.49	3.05	4.30
Gamma	0.60	0.01	20	52.5	43.0	51.5	1.94	1.59	1.94
Gaussian-like	0.60	0.01	4.47	68.0	58.4	66.2	2.72	2.30	2.57
Rectangular	0.60	0.01	0	21.5	20.8	21.5	0.67	0.65	0.67
Monodisperse	0.30	0.30	0	68.4	106.9	68.4	2.38	5.14	2.39
Bimodal Equal Concentration	0.1	0.6	0	14.6	14.8	14.6	0.44	0.43	0.44
Equal Power	0.1	0.6	—	560.4	48.1	—	44.1	1.82	—

useful. It might happen that the shape function itself may provide sufficient information. The formulation of a successful method, however, will ultimately depend on an increased understanding of the origin of axis ratio distributions, how they depend on drop size, and their characteristics under different meteorological conditions.

4. Some observations

Although it would be illuminating to apply (4), (7)–(11), (14)–(15) and Figs. 6–7 to actual data, this requires simultaneous measurements of Z_{DR}, Γ, ρ, and A_3, the one-way attenuation rate at a radar wavelength of 3.2 cm. Such data are not yet available.

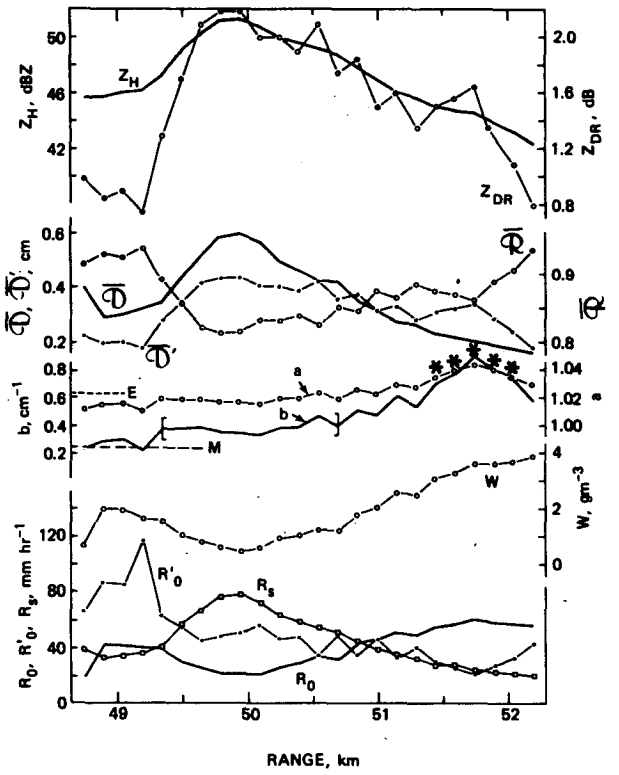

FIG. 8. Plot of dual-wavelength (10 and 3 cm) and differential reflectivity measurements as a function of range. The observations were collected at 1° elevation angle. The top two curves are horizontal reflectivity factor Z_H and differential reflectivity Z_{DR}. The curves labeled $\bar{\mathcal{D}}$ and $\bar{\mathcal{D}}'$ were estimated from the dual-wavelength and Z_{DR} data, respectively, (see text) while $\bar{\mathcal{R}}$ was calculated from Z_{DR}. The intercept a and slope b of linear shape functions were estimated using $\bar{\mathcal{D}}$ and $\bar{\mathcal{R}}$ (see text). The letters E and M correspond to the slopes of a linear shape function for equilibrium shaped drops and the Miami, Florida data (Fig. 1), respectively. The bottom curves labeled R_0 and W are the rainfall rate in still air and liquid water content, respectively, calculated from $\bar{\mathcal{D}}$. The curve R'_0 is calculated first using an average shape function to estimate $\bar{\mathcal{D}}'$ from Z_{DR} and then calculating the rainfall rate in still air. Curve R_s is the rainfall rate profile calculated using a Z–R relation (see text).

However, simultaneous dual-wavelength (10.71 and 3.21 cm) and differential reflectivity data were collected by the CHILL radar during a rainstorm in central Illinois in 1980 (Fig. 8). Data were collected over a 3.6 km length path centered about 51 km from the radar at less than 1 km AGL or some 2–3 km below the 0°C level. It is likely, therefore, that most, if not all, of the precipitation was liquid.

a. Path length averages

While Z_{DR} was computed every 150 m from reflectivity measurements at horizontal and vertical polarizations averaged for several seconds, the attenuation rate was estimated from the monotonic increasing component of log (Z_{10}/Z_3) as a function of range (Jameson, 1977), where the 10 and 3 denote the respective wavelengths and both reflectivity factors were measured using vertically polarized transmissions. Although this scheme appears to adequately estimate the *mean* 3 cm attenuation rate, $\bar{A}_3$, over several range bins, bin-by-bin (150 m) spatial resolution is not possible. Bin values of A_3 may accordingly be expected to deviate from $\bar{A}_3$.

In this case, $\bar{A}_3$ was estimated to be 0.51 dB km^{-1} (one-way) over 3.6 km distance. Over this path the average reflectivity factor measured with vertical polarization was Z_V = 46.2 dB(Z) and Z_{DR} = 1.74 dB, where Z_{DR} was computed from Z_V and Z_H. From (21) of Jameson (1983a), $\bar{\mathcal{R}}$ = 0.853, while from (8), $\bar{\mathcal{D}}$ = 0.358. The linear shape function inferred from these measurements is then $\bar{\mathcal{R}} = 1.02 - 0.48\bar{\mathcal{D}}$. This equation lies between equilibrium and that derived from drop camera observations in North Carolina (Fig. 1).

The mean values of W (15) and R_0 (14) along the entire path were 1.65 g m^{-3} and 41 mm hr^{-1}, respectively. Encouragingly, these values are within the range of measurements reported by penetration aircraft for convective storms. These mean values are also consistent with estimates using reflectivity–rainfall rate and reflectivity–water content relationships appropriate for thunderstorms. For example, using Z_V and relationships of Sekhon and Srivastava (1971), estimates of the mean values of W and R would be about 1.61 g m^{-3} and 39 mm hr^{-1}, respectively.

b. Bin-by-bin estimates

Bin-by-bin estimation of the meteorological variables is, in general, difficult. Under some circumstances, for example, it might be necessary to determine the raindrop shape function on a bin-by-bin basis. Although the polarization quantities and reflectivity factor can be measured at each bin, only the path length estimate of $\bar{A}_3$ is available. There are two

alternative options for attempting higher spatial resolution estimates. One is to assume that $\bar{A}_3$ is a sufficiently accurate representative value of the attenuation rate at each bin so that $\bar{\mathcal{D}}$ and the constants, a and b, of the linear shape function can be calculated. Alternatively, one may first determine the path length average shape function using $\bar{A}_3$ and the path length mean value of Z_{DR}, say, and then make estimates of the meteorological variables based on the polarization measurements alone. Whether or not either approach would provide meteorologically meaningful results is not known. One is free, however, to procede with a bin-by-bin analysis using either scheme.

1) Estimates of meteorological parameters using bin-by-bin estimates of the raindrop shape function

Although A_3 may differ from $\bar{A}_3$, there is consistent behavior in much of Fig. 8. At a range of just less than 49.5 km, Z_{DR} rises rapidly to a peak of about 2.20 dB at near 50.0 km. In that same region Z_H increases from 46 to 52 dB(Z). Meanwhile $\bar{\mathcal{R}}$ drops from ~0.94 to ~0.82 suggesting the presence of larger drops than $\bar{\mathcal{D}}$, which is estimated independently from $\bar{\mathcal{R}}$, confirms that suspicion, with $\bar{\mathcal{D}}$ increasing from about 0.32 to 0.59 cm. This coupling of $\bar{\mathcal{R}}$ and $\bar{\mathcal{D}}$ behavior extends for over 1.25 km and is largely responsible for an almost constant value of b over the path from 49.4 to 50.7 km (brackets on the curve for b). Over the entire path, however, b varied considerably. From 48.75 to ~51.0 km, values of the slope were consistent with the drop camera data (non-equilibrium shapes) while between 51.2 to 52.2 km the values of b suggest axis ratios that are approximately consistent with equilibrium values. At five locations (denoted by asterisks), the linear shape function becomes super-equilibrium, i.e., drops of diameter $\bar{\mathcal{D}}$ are more flattened than equilibrium theory would predict. Although this might occur if the precipitation were in part composed of melting subcentimeter ice particles that had flattened beyond equilibrium, these values could also be due to departures of the true A_3 from $\bar{A}_3$ or other problems. In any subsequent analysis, of course, caution would have to be exercised at these locations.

The structures of R_0 and W as functions of range are interesting. At the location of the largest values of Z_H and Z_{DR}, R_0 and W have actually decreased. This appears to be the result of a decrease in the number concentration relative to the preceding ranges. Since $\bar{\mathcal{D}}$ changed from 0.29 at 48.9 km to 0.58 at 49.8 km while Z_H only increased 5 dB(Z), the concentration decreased by approximately a factor of 20 in one kilometer. Even with this decrease in concentration, though, R_0 declined only by a factor of 2 because of the increased fall speed of the larger drops. On the other hand, W declined by over a factor of 3.

2) Estimates of meteorological parameters using a path length "average" raindrop shape function and the polarization measurements

The profile of $\bar{\mathcal{D}}'$, the estimate of mean reflectivity weighted diameter using polarization measurements and an average shape function, is quite similar to $\bar{\mathcal{D}}$ (Fig. 8) calculated from the previous approach. The two curves are not identical, however, and this provides interesting differences in the rainfall rate profile, R_0' from R_0 computed above. Insofar as reasonably reliable bin-by-bin estimates are possible, differences such as these may prove useful in selecting one of these two bin-by-bin analysis approaches.

The rainfall rate profiles deduced by either of these techniques are both distinctly different from the profile R_s calculated from the Z–R relation of Sekhon and Srivastava (1971) using an average reflectivity factor $(Z_H + Z_V)/2$. In Z–R relations, R is a monotonic increasing function of Z so that the peak in the estimated rainfall rate is necessarily coincident with the reflectivity maximum. Consequently in Fig. 8 the maximum in R_s is coincident with smaller values of R_0 and R_0'.

To summarize, this example is encouraging since it shows that the derived techniques can produce logical and consistent results from actual data. Direct verification of the techniques, of course, would require in situ measurements of the drop distribution and raindrop shape functions over significant portions of the radar pulse volume. In the absence of such data, alternative explanations of the observations are always possible.

5. Summary and conclusions

In another paper (Jameson, 1983a), it was shown that either Z_{DR} or the combination of ρ and Γ can yield estimates of the radar reflectivity weighted mean axis ratio $\bar{\mathcal{R}}$. It was also shown that the radar power weighted variance of the axis ratio $\sigma^2_{\mathcal{R}}$ could be extracted from the combination of ρ and Γ.

This paper defines a method for independently determining the reflectivity weighted average drop size $\bar{\mathcal{D}}$ by dual wavelength (10.7 and 3.2 cm) radar measurements. The combination of $\bar{\mathcal{R}}$ and $\bar{\mathcal{D}}$ can be used to define a shape function, i.e., the relation between mean axis ratios and drop diameters. As long as the correspondence between the mean axis ratios and drop diameters is one-to-one, it is possible to convert a measurement of $\bar{\mathcal{R}}$ to $\bar{\mathcal{D}}$ and $\sigma^2_{\mathcal{R}}$ to $\sigma^2_{\mathcal{D}}$.

With only $\bar{\mathcal{D}}$ and $\sigma^2_{\mathcal{D}}$ available from radar power measurements, for many drop size distributions it is

not possible to distinguish one analytic form of the drop size distribution from another. The measurement of higher reflectivity weighted moments such as skewness are probably needed to help sort out particular analytic forms of drop size distributions. For many observed forms of drop size distributions, however, the skewness is small, and in those cases $\bar{\mathcal{D}}$ and $\sigma_{\mathcal{D}}^2$ may provide most of the available meteorological information.

Estimators of the rainfall rate in still air R_0 and rainwater content W were constructed using a wide variety of drop size distributions (e.g., exponential, gamma, Gaussian-like, rectangular, monodisperse, and others) and drop shape functions. Using only $\bar{\mathcal{D}}$, values of R_0 ranged by at most ±36% of the estimated R_0 while W varied by at most ±54%. Although estimates of R_0 and W could be improved further if a radar measure of μ_3 could be devised, for many drop size distributions use of both $\bar{\mathcal{D}}$ and $\sigma_{\mathcal{D}}$ apparently exploits much of the available meteorological information and, potentially, can yield significantly improved estimates of R_0 and W.

The realization of this potential improvement requires progress in at least two areas. First, if natural raindrops of a particular size possess a single, unique axis ratio, then Figs. 6–7 have immediate application. If, on the other hand, raindrops of a particular size exhibit a wide variety of axis ratios, a means for subtracting the contribution of this variation of shape from $\sigma_{\mathcal{R}}^2$ must be found. If future research indicates that the contribution of the spread in the drop size distribution to $\sigma_{\mathcal{R}}^2$ may be identified, then the necessary $\sigma_{\mathcal{D}}^2$ can be extracted for implementation of Figs. 6–7.

Meteorological variables are amazingly complex. The future understanding of these complexities will require the full simultaneous use of all currently available and future remote measurements. To be generally useful, however, these measurements will have to be collected rapidly in a few seconds to a few minutes over large volumes. The full potential of current radar polarization techniques are not likely to be realized until rapid polarization measurements are possible.

Acknowledgments. The author is greatly indebted to Dr. Charles Warner at the University of Virginia for providing the program used to calculate the raindrop scattering functions used in much of this work. A 1978 report to the Alberta Research Council by Dr. Warner entitled "Calculated Scattering Characteristics of Hailstones at Weather Radar Wavelengths" describes an improved and shortened calculation procedure. I thank Dr. David B. Johnson of the Illinois State Water Survey for his time and invaluable comments. This work was supported by the National Science Foundation under Grants NSF ATM79-18365 and NSF ATM81-08455.

REFERENCES

Atlas, D., 1954: The estimation of cloud parameters by radar. *J. Meteor.*, **11**, 309–317.

——, and C. W. Ulbrich, 1974: The physical basis for attenuation-rainfall relationships and the measurement of rainfall relationships and the measurement of rainfall parameters by combined attenuation and radar methods. *J. Rech. Atmos.*, **8**, 275–298.

——, and ——, 1977: Path and area-integrated rainfall measurement by microwave attenuation in the 1–3 cm band. *J. Appl. Meteor.*, **16**, 1322–1331.

Beard, K. V., D. B. Johnson and A. R. Jameson, 1983: Collisional forcing of raindrop oscillation. *J. Atmos. Sci.*, **40**, 455–462.

Bresch, J. F., 1982: Raindrop axis ratios. Masters thesis, Dept. Atmos. Sci., University of Illinois, 60 pp.

Brook, M., and D. J. Latham, 1968: Fluctuating radar echo: Modulation by vibrating drops. *J. Geophys. Res.*, **73**, 7137–7144.

Eccles, P. J., and E. A. Mueller, 1971: X-band attenuation and liquid water content estimation by a dual-wavelength radar. *J. Appl. Meteor.*, **10**, 1252–1259.

Gans, R., 1912: Über die form ultramikroshopischer Goldteilchen. *Ann. Phys.*, **37**, 881–900.

Goddard, J. W., F. S. M. Cherry and V. N. Bringi, 1982: Comparison of dual-polarization radar measurements with ground-based distrometer measurements. *J. Appl. Meteor.*, **21**, 252–256.

Hall, M. P. M., S. M. Cherry, J. W. F. Goddard and G. R. Kennedy, 1980: Raindrop sizes and rainfall rate measured by dual-polarization radar. *Nature*, **285**, 195–198.

Hendry, A., and G. C. McCormick, 1974: Polarization properties of precipitation particles related to storm structure. *J. Rech. Atmos.*, **8**, 189–200.

——, —— and B. L. Barge, 1976: The degree of common orientation of hydrometeors observed by polarization diversity radars. *J. Appl. Meteor.*, **15**, 633–640.

Humphries, R. G., and B. L. Barge, 1979: Polarization and dual-wavelength radar observations of the bright band. *I.E.E.E. Trans. Geosci. Electron.*, **GE-17**, 190–195.

Jameson, A. R., 1977: A dual-wavelength study of a hailstorm. Ph.D. dissertation, Dept. Geophys. Sci., University of Chicago, 179 pp.

——, 1983a: Microphysical interpretation of multiparameter radar measurements in rain: Part I: Interpretation of polarization measurements and estimation of raindrop shapes. *J. Atmos. Sci.*, **40**, 448–454.

——, and K. V. Beard, 1982: Raindrop axial ratios. *J. Appl. Meteor.*, **21**, 257–259.

McCormick, G. C., and A. Hendry, 1975: Principles for the radar determination of the polarization properties of precipitation. *Radio Sci.*, **10**, 421–434.

——, and ——, 1976: Polarization related parameters for rain: Measurements obtained by radar. *Radio Sci.*, **11**, 731–740.

——, —— and B. L. Barge, 1972: The anisotropy of precipitation media. *Nature*, **238**, 214–216.

Pruppacher, H. R., and K. V. Beard, 1970: A wind tunnel investigation of the internal circulation and shape of water drops falling at terminal velocity in air. *Quart. J. Roy. Meteor. Soc.*, **96**, 247–256.

Sekhon, R. S. and R. C. Srivastava, 1971: Doppler radar observations of drop-size distributions in a thunderstorm. *J. Atmos. Sci.*, **28**, 983–994.

Seliga, T. A., and V. N. Bringi, 1976: Potential use of radar differential reflectivity measurements at orthogonal polarizations for measuring precipitation. *J. Appl. Meteor.*, **15**, 69–76.

Ulbrich, C. W., and D. Atlas, 1978: The rain parameter diagram: Methods and applications. *J. Geophys. Res.*, **83**, 1319–1325.

Wexler, R., and D. Atlas, 1963: Radar reflectivity and attenuation of rain. *J. Appl. Meteor.*, **2**, 276–280.